EUROPEAN ORGANIZATION FOR NUCLEAR RESEARCH

Proposal to the ISOLDE and Neutron Time-of-Flight Committee

Emission Mössbauer spectroscopy of topological kagome magnets

[10th of January 2024]

Roberto Mantovan[1], Anastasios Markou[2,3], Edouard Lesne[3], Claudia Felser[3], Haraldur Pall Gunnlaugsson[4], Hilary Masenda[5], Juliana Schell[6,7], Ian Chang Jie Yap[7], Adeleh Mokhles Gerami[6,8], Carlo Grazianetti[1], and The Mössbauer collaboration at ISOLDE/CERN[9]

[1] *CNR-IMM, Unit of Agrate Brianza, Via C. Olivetti 2, 20864 Agrate Brianza (MB), Italy*
[2] *Department of Physics, University of Ioannina, 45110 Ioannina, Greece*
[3] *Max Planck Institute for Chemical Physics of Solids, Nöthnitzer Str. 40, 01187 Dresden, Germany*
[4] *Science Institute, Univ. Iceland, 107-Reykjavik, Iceland*
[5] *School of Physics, University of the Witwatersrand, Johannesburg 2050, South Africa*
[6] *European Organization for Nuclear Research (CERN), CH-1211 Geneva, Switzerland*
[7] *Institute for Materials Science and Center for Nanointegration Duisburg-Essen (CENIDE), University of Duisburg-Essen, 45141 Essen, Germany*
[8] *School of Particles and Accelerators, Institute for Research in Fundamental Sciences (IPM), P.O. Box 19395-5531, Tehran, Iran*
[9] ISOLDE, European Organization for Nuclear Research (CERN), CH-1211 Geneva, Switzerland (https://e-ms.web.cern.ch/content/collaborators)

Spokespersons: Roberto Mantovan, roberto.mantovan@cnr.it;
Edouard Lesne, edouard.lesne@cpfs.mpg.de
Contact person: Juliana Schell (juliana.schell@cern.ch)

CERN-INTC-2024-004 / INTC-P-687
10/01/2024

Abstract: The so-called 'kagome' lattices are made by two-dimensional (2D) lattices of corner-sharing triangles, consisting of 3d transition metal atoms (T: Fe, Mn, Co) with space-filling atoms (X: Sn, Ge) at the centre of the hexagon, to form binaries T_mX_n compounds. They typically show the simultaneous existence of Dirac fermions, flat bands and van Hove singularities in their electronic structures. Such a rich interplay between topology and correlated phenomena, provides interesting platforms towards unconventional magnetic and/or superconducting states, making kagome magnets extremely attracting for a wide range of applications. As of today, several open

fundamental questions are unresolved, requiring a deep understanding of the atomic scale chemical, structural and magnetic properties of T_mX_n materials. Within this proposal we aim at addressing some of them, by making use of emission Mössbauer spectroscopy at ISOLDE/CERN with the help of radioactive ^{57}Mn and ^{119}In probes.

Summary of requested shifts: 11 shifts (split into 3 runs over 2 years)

1 Motivation

In solid-state systems, electron correlation plays a crucial role in determining physical properties, leading to various quantum phases with broken symmetry [1]. Correlated systems, where Coulomb interactions are significant (compared to the kinetic energy of electrons), are known to exhibit superconductivity, metal-insulator Mott transition, complex magnetism (noncollinear, noncoplanar, etc.), charge and spin density waves as well as nematic orders and other collective quantum phenomena. The competition and interplay of these phases is observed for instance in the famously known high-T_C cuprate superconductors [2], and recently extends to the family of **topological kagome magnets** (TKM), with their reported and potentially unconventional magnetic and superconducting ground states [3, 4]. The so-called 'kagome' lattice is a two-dimensional (2D) lattice of corner-sharing triangles, consisting of 3d transition metal atoms (T: Fe, Mn, Co) with space-filling atoms (X: Sn, Ge) at the centre of the hexagon, Fig.1(a). The tight-binding band structure of kagome lattice typically exhibit Dirac points (DP) at the K-point, van Hove singularities (vHs) at the M-point, and a flat band (FB) across the whole Brillouin zone, Fig.1(b). The simultaneous existence of Dirac fermions, FB and vHs in their electronic structures, makes TKM intriguing platforms to jointly study and exploit topology, correlated phenomena such as magnetism, and potential instabilities towards long-range many-body orders [3]. As displayed in Fig.1(c-e), the binary kagome metal series T_mX_n has stacking series with m:n = 3:1, 3:2 and 1:1. The structural dimensionality decreases with increasing ratio of X to T: in the TX (1:1) (Fig.1(e)) structure the kagome layers are perfectly aligned with one another and are interleaved with S layers, while in the T_3X structure (Fig. 1(c)), neighbouring kagome layers are directly stacked without spacing layers. In the T_3X_2 structure (Fig. 1(d)), both types of stacking coexist.

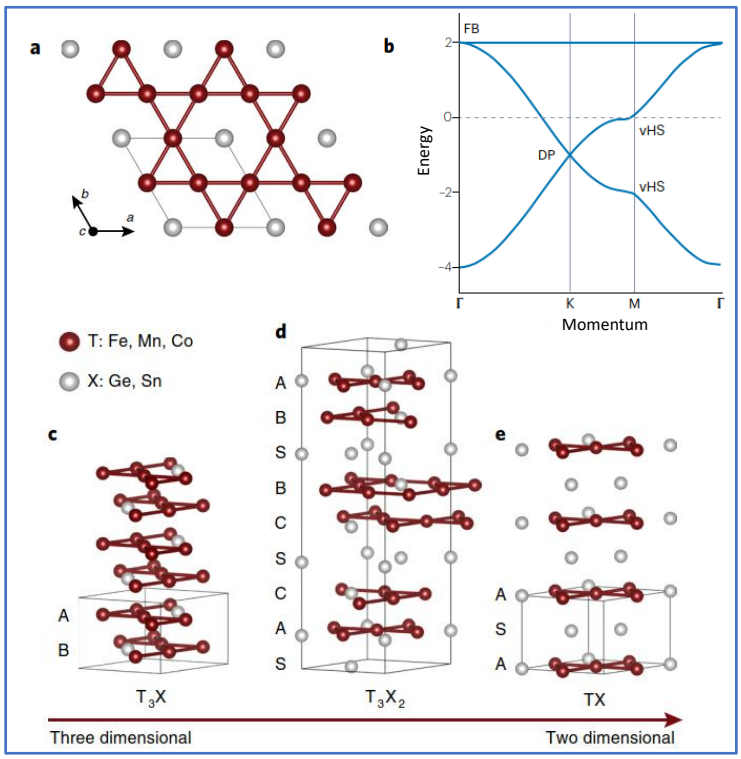

***Fig. 1**. Crystal structure of binary kagome metals T_mX_n. (a) Top view of the kagome network, which consists of 3d transition metal atoms (T: Fe, Mn, Co) with space-filling atoms (X: Sn, Ge) at the centre of the hexagon; (b) Tight-binding band structure of kagome lattice* (see text); *(c–e) Stacking sequences of T_mX_n with m:n = 3:1 (c), 3:2 (d) and 1:1 (e). (Figure is adapted from Refs. [4, 5]).*

TKM have been identified as promising materials for high-efficiency and low-power consumption in next-generation memory applications [6]. Therefore, the kagome lattice

and its associated materials offer an unparalleled opportunity for fundamental research with new physics and development of various technological applications. In particular, **our interest is in the following TDK: Fe_3Sn_2, Fe_3Sn, and Mn_3Sn**.

Fe_3Sn_2 has a hexagonal crystal structure with space group R-3m and lattice constants of a=5.338 Å and c=19.789 Å. It contains a stanene layer that is sandwiched between Fe_3Sn kagome bilayers, as shown in Fig. 1(d). Fe_3Sn_2 is a soft magnet exhibiting strong in-plane magnetization induced by FB [7]. Interestingly, Fe_3Sn_2 has topological properties in both momentum and real-space. Photoemission and tunnelling experiments revealed the existence of DP and a kagome bilayer electronic structure [8,9]. Additionally, it shows a sizable anomalous Hall effect, stemming from the nonzero Berry curvature associated with the DP. Another intriguing physical phenomenon observed in Fe_3Sn_2 is the detection of nematicity, which is strongly related to correlated electrons. In addition, during the demagnetization process following saturation, a complex spin texture gives rise to skyrmions and a topological Hall effect [10, 11]. Finally, spin-reorientation occurs in Fe_3Sn_2 at low temperature (see [12] and refs therein), which may be important in skyrmions formation [10], but its nature is still debated.

The kagome magnet **Fe_3Sn** has a hexagonal $D0_{19}$-type structure and space group of P63/mmc, which is the same as the antiferromagnetic Weyl semimetals Mn_3Sn (Fig 1(c)). Although less explored compared to Fe_3Sn_2, Fe_3Sn exhibits large anomalous Hall and Nernst effects [13, 14] due to Weyl nodes as predicted by theoretical calculations. Some controversies are still open about magnetic anisotropy in Fe_3Sn [15]. As a note, both Fe_3Sn_2 and Fe_3Sn TDK thin films are far less explored when compared to their bulk form.

Mn_3Sn is a strongly correlated antiferromagnet displaying room temperature zero-field anomalous Hall effect [16]. A recent report about the tuning of topological properties in Mn_3Sn via Fe doping, appeared [17], where the authors report about the electronic, magnetic, and topological properties of $Mn_{3-x}Fe_xSn$ single crystals (x=0÷0.35), showing that the magnetic properties can largely be affected by Fe doping. Moreover, uniaxial magnetocrystalline anisotropy is induced by Fe, which in combination with competing magnetic interactions can produce nontrivial spin texture (i.e. skyrmions). Emission Mössbauer spectroscopy (eMS) at ISOLDE is a unique way to conduct Fe-Mössbauer spectroscopy in this alloy.

2 Preliminary results

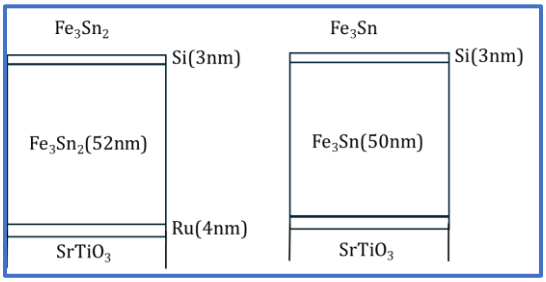

***Fig. 2**. The two samples used for testing, labelled Fe_3Sn_2 and Fe_3Sn provided by the group of Prof. C. Felser at MPI-D [18].*

To test the feasibility of using $^{57}Fe/^{57}Mn$-eMS in TKM, test experiments were performed during the Mn beamtime in September 2023 on the two samples pictured in Fig. 2, which we indicate as Fe_3Sn_2 and Fe_3Sn in the following. Samples have been pre-characterized by X-ray

diffraction (not shown), which showed only minor differences between the two phases. The eMS was performed on the daughter ^{57}Fe following implantation of ^{57}Mn ($T_{½}$ = 1.5 min.). The dominating part of the implanted ^{57}Mn resides in the Fe_3Sn_2 and Fe_3Sn layers, as suggested by TRIM simulations (not shown) that shows an ion range of ≥ 20 nm for both samples. Figure 3(a, b) depicts the eMS of Fe_3Sn_2 and Fe_3Sn, respectively, while Fig. 3(c) shows the CEMS of Fe_3Sn_2 as recorded on the same sample, after the eMS experiment. Based on Fig. 3, we make three immediate conclusions, which are of paramount importance to justify the present proposal:

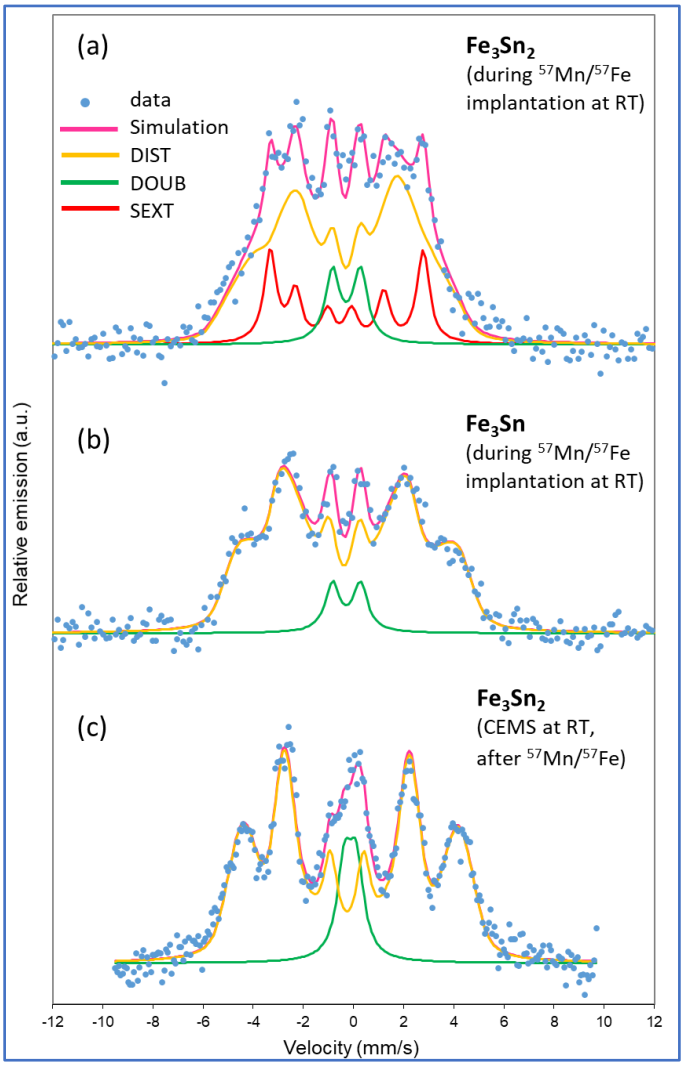

Fig 3. eMS spectrum of (a) Fe_3Sn_2, (b) Fe_3Sn, and (c) CEMS spectrum of Fe_3Sn_2, all recorded at room temperature. CEMS data has been recorded following eMS on the same sample measured at ISOLDE (a), and following annealing at 200 °C to recover implantation-induced damage.

1. The **^{57}Mn-implantation-induced damage does not prevent the observation of clear magnetic components even at room temperature**, see Fig. 3(a, b). Both samples show very clear magnetically-split structures. This is not straightforward, since in the past, it was quite harsh to gather information about magnetic hyperfine splitting in binaries Heusler alloys such as Mn-Ga [19]. Due to the potential technological relevance of these materials, it is important to be able to probe them and gather useful information already at room temperature.
2. **^{57}Mn eMS is sensitive to stoichiometry of the TKM**. Apart from exploring the Fe_3Sn properties, such a difference will be helpful to gather atomic-scale information in Fe_3Sn_2, in which the kagome Fe_3Sn is one of the building-blocks (Fig. 1).
3. The CEMS of Fe_3Sn_2 in Fig. 3(c) is very different than the corresponding eMS spectrum in Fig. 3(a), evidencing that **eMS appears to be useful to gather additional insight into the magnetic nature of Fe_3Sn_2, when compared to home-lab CEMS.**

The Fe_3Sn_2 eMS data can be interpreted with 3 separate spectral components indicated with DIST, DOUB and SEXT, while Fe_3Sn and CEMS of Fe_3Sn_2 shows only the presence of a DIST and DOUB components. Within this preliminary analysis, we use a unique DIST and

DOUB for all the measurements shown in Fig. 3, even if the hyperfine parameters are not always identical. Several Mössbauer studies on Fe-Sn bulk materials are available, since there was some interest in some of them during the 70's-80's, mainly as rare-earth free permanent magnets [20-22], but studies on thin films are scarce and limited to multilayers [23] or very thick layers, i.e. μm-range [24]. We are aware of only one CEMS study on Fe-Sn layers below 100 nm thickness [25], where FeSn formed upon ion beam mixing. From one hand, the interpretation of our data could take the advantage of what was previously done in bulk materials. On the other hand, we have opportunities to be the first group presenting a **detailed atomic-scale view of these materials in their thin film form**. In Palchucán *et al.*, [15] and Echevarria-Bonet *et al.* [26], Fe_3Sn crystals were investigated, and the hyperfine parameters were very similar to those we observe for the DIST component in our Fe_3Sn system (Fig.3(b)), which presents an isomer shift $\delta \sim 0.3$mm/sec and an average hyperfine magnetic field $B_{hf} \sim 22$ T. Among others, Fe_3Sn_2 crystals have been studied in [20, 21], with observed hyperfine parameters in accordance with what we extract for the DIST component in Fe_3Sn_2 (Fig. 3(a)), with $\delta \sim 0.4$ mm/sec and $B_{hf} \sim 20$ T. The immediate most **striking difference between the eMS of Fe_3Sn_2 when compared to Fe_3Sn, is the presence of the additional relatively sharp magnetically-split sextet (with $\delta \sim$ 0.4mm/sec and $B_{hf} \sim 19$ T) indicated with "SEXT" in Fig. 3(a), which does not appear in CEMS, Fig. 3(c)**. This is surprising, since Fe_3Sn_2 should show a single magnetic component due to the presence of a unique crystallographic Fe site [21], see also Fig. 1. The overall shape of the CEMS spectrum of Fe_3Sn_2 appears very similar to the eMS of Fe_3Sn (Fig. 3). Quite intriguingly, this could suggest that the additional SEXT component observed by eMS in Fe_3Sn_2, may originate from Mn/Fe somewhere probing the stanene-Sn_2 layers in the Fe_3Sn_2 structure (Fig. 1). If confirmed, this may be a relevant discovery, since it could suggest the possibility to magnetize stanene, something that has been so far only theoretically predicted [27]. The reason for the difficulties in obtaining magnetism in stanene is mainly that pure Sn_2 is unstable at ambient conditions, and this makes quite challenging to conduct 3d-element doping experiments. The **possibility to create and probe magnetic stanene in Fe_3Sn_2, could be quite a unique opportunity for eMS at ISOLDE.** By eMS we also have direct access to angle between the samples' magnetization and the film plane by measuring the relative ratio between the middle and inner lines of a magnetically-split sextet [28]. Since there is still some controversies on the nature of the Fe_3Sn anisotropy (see Ref.[15] and refs therein), this is an additional physics of interest that we can address by monitoring and comparing data in the pure Fe_3Sn with that from the Fe_3Sn kagome layers within Fe_3Sn_2.

3 Proposed studies

For each system, we plan to use at least 2 samples. In particular, we are interested in probing the role of two different buffer layers (Ru, Pt) for the Fe_3Sn compound, since we anticipate that these two buffer layers will play a role in stabilizing the different strain states, i.e. Fe_3Sn is expected to be compressively strained by -1.2% *vs* tensely strained by + 0.85%, when grown on Pt *vs* Ru buffer layers respectively. For all systems, we plan TKM

layers' thickness in the range of 30 ÷ 100 nm. Thicker TKM (>80 nm) will tend towards their bulk lattice parameters due to strain relaxation, while intermediate thicknesses will likely show some strain gradient. According to TRIM simulations, with eMS we're mostly sensitive to the first 20 ÷ 30 nm closer to the surface, meaning that by comparing experiments in TDK of ~30 nm and >80 nm, we will probe the influence of structural distortions on the hyperfine parameters, an information hardly accessible with conventional CEMS. In particular, direct information on the effect of strain on the TDK could be obtained from the relative intensities of lines 2 and 5 of the "DIST" component seen in Fe-Sn (Fig. 3), similarly as previously done by some of us on Fe/V superlattices [29]. We will also conduct experiments on Fe_3Sn_2 thin films produced by molecular beam epitaxy (MBE) at CNR-IMM Unit of Agrate Brianza, where there is an interest in using them for quantum computations [30]. It will be of high technological interest to compare Fe_3Sn_2 as produced with two different thin film depositions' methods. Table 1 summarizes the estimated time to be spent for each sample during ^{57}Mn-eMS experiments, by making use of the different HT-lid, LT-lid, and ROT-lid sample's lids available in the eMS setup (details follow).

***Table 1**. Sample list to be measured by ^{57}Mn-eMS, and estimated time to be spent for each sample by using the different lids: HT-lid, LT-lid, ROT-lid. All samples will be capped, i.e. with Si.*

System to be studied (thickness in parentheses)	***number of samples***	***hours with HT-lid***	***hours with LT-lid***	***hours with ROT-lid***
substrate/buffer(Ru, ≤4nm)/**Fe_3Sn_2** (≥50nm)/capping(≤3nm), sputtering	≥2 (at least 2 thicknesses)	5	4	6
substrate/buffer(Ru, Pt ≤4nm)/**Fe_3Sn** (≥50nm)/capping(≤3nm), sputtering	≥2 (at least 1 per each buffer)	5	4	6
substrate/buffer(Ru ≤4nm)/**Mn_3Sn** (≥50nm)/capping(≤3nm), sputtering	≥2 (at least 2 thicknesses)	5	4	6
substrate/buffer(Ru, Pt ≤4nm)/**Fe_3Sn_2**/capping, MBE	≥2 (at least 2 thicknesses or buffer)	5	4	6

The experimental plan leads to a total of 60 hours, i.e. 7.5 shifts of ^{57}Mn. To these we add 1.5 shifts for calibration and "opportunistic" experiments, leading to a **total of 9 requested shifts of ^{57}Mn**. Additionally, we **request 2 shifts of ^{119}In**, foreseeing 0.5 shift per each sample type listed in Table 1. In Fe_3Sn_2 the Sn atoms occupies two non-equivalent crystallographic sites [21]. It would be important to monitor magnetic polarization at the Sn site within the stanene-Sn_2 layers and to correlate with the SEXT component observed by ^{57}Mn-eMS, Fig. 3(a), as we previously succeeded in Mn-Ga alloys [19].

HT-lid: allows mounting 4 samples at once, and to perform eMS measurements from room temperature up to 600-700 K. It will allow a full characterization of samples' magnetism at the most atomic-scale up to their Curie temperature. To carefully follow (and compare) the evolution of the DIST and SEXT components in Fe_3Sn_2 and Fe_3Sn will be fundamental to get insight into the nature of SEXT observed in Fe_3Sn_2 (Fig. 3(a)).

LT-lid: allows mounting 1 sample at once, to perform eMS from room temperature down to ~100 K. We will follow the hyperfine magnetic field evolution to complete studies done

with HT-lid. Additionally, these experiments will give important hints about the atomic-scale origin of spin reorientation processes [12].

ROT-lid: allows to mount 1 sample to perform eMS (with or without an applied magnetic field of ~0.6 T), allowing angular-dependent measurements to unambiguously determine the nature of magnetic interactions [31, 32], to study the magnetic anisotropies of the TKM, and to determine site symmetry of paramagnetic doublets.

In general, through T-dependent eMS we will assess the chemical composition and homogeneity of the developed TDK thin films, ensuring that the desired phases are present in the material. Moreover, we will gather information about the local electronic structure in Fe_3Sn_2, Fe_3Sn, and Mn_3Sn around the constituent Fe(or Mn) and Sn nuclei. We will determine the nature of defects in TDK, distinguishing between slow paramagnetic relaxations (no change in B_{hf} with temperature) and/or determine at the atomic-scale the strength of long-ranged magnetic interaction (i.e. Curie T), and we'll determine the nature of sites (substitutional, interstitial, …). The studies will be compared with magnetic measurements conducted via SQUID and/or VSM to serve as the basis to understand the origin for the differences observed macroscopically. Before eMS experiments, all the samples will be characterized by X-Ray Diffraction and X-Ray Reflectivity, to ensure about the crystalline quality and the epitaxial relationships of the layers, as well as to accurately verify their thickness. Selection of studies will be also conducted after the implantation. Certainly, CEMS will be conducted on all Fe-based implanted samples both before and after eMS. The comparison among (i) CEMS before eMS, (ii) eMS, and (iii) CEMS after eMS, will provide the most comprehensive atomic-scale study that can be done in the selected TKM.

We will perform DFT simulations to calculate electric field gradient and electron density of Fe and Sn in Fe_3Sn_2, Fe_3Sn, and Mn_3Sn, focusing on various Fe and Sn sites and configurations of defect complexes around them, in order to univocally determine the nature of the observed magnetic components. Full potential linearized augmented plane wave (FP-LAPW) method as implemented in the WIEN2K code [33], will be employed for optimizing the structural lattice parameters of the cell and to compute the hyperfine parameters. The routine employed in the calculation for the determination of Mössbauer parameters are detailed in Refs. [34,35].

4 Summary

To summarize, by making use of the requested 11 shifts, **we aim at addressing the following open scientific issues**:

A) Can we induce magnetic ordering in the Sn_2-stanene layers in Fe_3Sn_2?
B) What is the atomic-scale origin of spin reorientation in Fe_3Sn_2 thin films?
C) What is the atomic-scale origin of the magnetic anisotropy in Fe_3Sn and Mn_3Sn?
D) What is the effect of dilute Fe-doping on the magnetic anisotropy in Mn_3Sn?
E) What is the effect of dimensionality (i.e. TKM' thickness) on the electronic and magnetic properties of TKM?

References

[1] S. Paschen *et al.*, Nat. Rev. Phys. 3, 9 (2021)

[2] E. Fradkin *et al.*, Rev. Mod. Phys. 87, 457 (2015)

[3] J. X. Yin *et al.*, Nature 612, 647 (2022)

[4] Y. Wang *et al.*, Nat. Rev. Phys. 5, 635 (2023)

[5] M. Kang *et al.*, Nat. Mater. 19, 163 (2020)

[6] H. Tsai *et al.*, Nature 580, 608 (2020)

[7] Z. Lin, *et al.*, Phys. Rev. Lett. 121, 096401 (2018)

[8] L. Ye *et al.,* Nature 555, 638 (2018)

[9] J. X. Yin *et al.,* Nature 562, 91 (2018)

[10] Z. Hou *et al.*, Adv. Mater. 29, 1701144 (2017)

[11] Q. Wang *et al.*, Chin. Phys. B 29, 017101 (2020)

[12] K. Heritage *et al.*, Adv. Funct. Mater. 30, 1909163 (2020)

[13] T. Chen *et al.*, Sci. Adv. 8, 1480 (2022)

[14] B. P. Belbase *et al.*, Phys. Rev. B 108, 075164 (2023)

[15] C. A. Palchucan *et al.,* Hyp. Interact. 241, 42 (2020)

[16] S. Nakatsuji *et al.*, Nature 527, 212 (2015)

[17] A. Low *et al.*, Phys. Rev. B 106, 144429 (2022)

[18] https://www.mpg.de/149744/chemical-physics-of-solids

[19] I. Unzueta *et al.*, Phys. Status Solidi B 259, 2200121 (2022)

[20] S. Ichiba *et al.*, Bulletin of the Chemical Society of Japan, 41, 2791 (1968)

[21] G. Le Caer *et al.*, Phys. F: Met. Phys. 8, 323 (1978)

[22] B. Rodmacq *et al.*, Phys.Rev. B 21,1911 (1980)

[23] S. El Khiraoui *et al.*, J. Supercond. Nov. Magn. 26, 3253 (2013)

[24] A. K. Zhubaev *et al.*, J. Phys.: Conf. Series 1923, 012009 (2021)

[25] J. H. Sanders *et al.*, J. Appl. Phys. 67, 3192 (1990)

[26] C. Echevarria-Bonet *et al.*, J. All. Comp. 769, 843 (2018)

[27] Dan-Xu Xing *et al.*, Superlattices and Microstructures 103, 139 (2017)

[28] P. Gutlich, "*Mössbauer Spectroscopy and Transition Metal Chemistry: Fundamentals and Application*", edited by P. Gütlich, E. Bill, and A.X. Trautwein (Springer, Berlin Heidelberg, Berlin, 2011)

[29] T. E. Mølholt *et al.*, Crystals 12, 961 (2022)

[30] PNRR MUR project PE0000023-NQSTI; https://www.nqsti.it
[31] H. P. Gunnlaugsson *et al.*, Appl. Phys. Lett. 97, 142501 (2010)
[32] H. P. Gunnlaugsson *et al.*, Hyperfine Interact. 197, 43 (2010)
[33] P. Blaha *et al.*, J. Chem. Phys. 152, 074101(2020)
[34] R., Mantovan *et al.* Sci Rep 7, 8234 (2017)
[35] H. P. Gunnlaugsson *et al.,* Physical Review B 106, 174108 (2022)

5. Details for the Technical Advisory Committee

5.1 General information

Describe the setup which will be used for the measurement. If necessary, copy the list for each setup used.

☒ Permanent ISOLDE setup: GLM beam line

☒ To be used without any modification

☐ To be modified: *Short description of required modifications.*

☒Travelling setup (*Contact the ISOLDE physics coordinator with details.*)

☒ Existing setup, used previously at ISOLDE: Emission Moessbauer Spectrometer from Ilmenau (eMIL).

☐ Existing setup, not yet used at ISOLDE: *Short description*

☐ New setup: *Short description*

5.2 Beam production

For any inquiries related to this matter, reach out to the target team and/or RILIS (please do not wait until the last minute!). For Letters of Intent focusing on element (or isotope) specific beam development, this section can be filled in more loosely.

- Requested beams:

Isotope	Production yield in focal point of the separator (/μC)	Minimum required rate at experiment (pps)	$t_{1/2}$
Isotope 1 Isotope 2 Isotope 3	^{57}Mn: 1.5x10^{8} at/µC ^{119}In: 2-3x10^{8} at/µC	^{57}Mn 1x10^{8} at/µC ^{119}In: 1.x10^{8} at/µC	1.5 min 2.4 min

- Full reference of yield information (*yield database for ^{57}Mn and IS630 for ^{119}In*)
- Target - ion source combination: UC_x with RILIS
- RILIS? (*Yes for element ^{57}Mn*)

  ☐ Special requirements: (*isomer selectivity, LIST, PI-LIST, laser scanning, laser shutter access, etc.*)

- Additional features?

☐Neutron converter: (*for isotopes 1, 2 but not for isotope 3.*)

☐ Other: (*quartz transfer line, gas leak for molecular beams, prototype target, etc.*)

- Expected contaminants: *Isotopes and yields*
- Acceptable level of contaminants: By using RILIS, no significant contaminants are expected.
- Can the experiment accept molecular beams? No.
- Are there any potential synergies (same element/isotope) with other proposals and LOIs that you are aware of? IS630, IS681, IS683, IS670.

5.3 HIE-ISOLDE

For any inquiries related to this matter, reach out to the ISOLDE machine supervisors (please do not wait until the last minute!).

- HIE ISOLDE Energy: *(MeV/u); (exact energy or acceptable energy range)*

  ☐ Precise energy determination required

  ☐ Requires stable beam from REX-EBIS for calibration/setup? *Isotope?*

- REX-EBIS timing

  ☐ Slow extraction

  ☐ Other timing requests

- Which beam diagnostics are available in the setup?
- What is the vacuum level achievable in your setup?

5.4 Shift breakdown

The beam request only includes the shifts requiring radioactive beam, but, for practical purposes, an overview of all the shifts is requested here. Don't forget to include:

- Isotopes/isomers for which the yield need to be determined

- Shifts requiring stable beam (indicate which isotopes, if important) for setup, calibration, etc. Also include if stable beam from the REX-EBIS is required.

An example can be found below, please adapt to your needs. Copy the table if the beam time request is split over several runs.

Summary of requested shifts:

With protons	Requested shifts
Yield measurement of isotope 1 Optimization of experimental setup using isotope 2 Data taking, isotope 1 → Data taking, isotope 2 → Data taking, isotope 3 Calibration using isotope 4	 ^{57}Mn: 9 shifts including calibration ^{119}In: 2 shifts including calibration
Without protons	Requested shifts
Stable beam to GLM beam line Background measurement	2 shifts maximum 0.5 shift for stable beam for every beam time with ^{135}Cs, ^{39}K or ^{55}Mn to GLM beam line. At least 90% of transmission expected at the Faraday cup of eMIL (traveling setup at the GLM beam line)

5.5 Health, Safety and Environmental aspects

5.5.1 Radiation Protection

• If radioactive sources are required:

- Purpose? Online experiment with ^{57}Mn and ^{119}In.
- Isotopic composition? ^{57}Mn and ^{119}In.
- Activity? 300 MBq online with no manipulation. Manipulation with only 30 kBq according to the existing and approved procedure.
- Sealed/unsealed? Unsealed.

- For collections:
  - Number of samples? 10-12 (including calibration ones)
  - Activity/atoms implanted per sample? 300 MBq online with no manipulation. Manipulation with only 30 kBq according to the existing and approved procedure.
  - Post-collection activities? (*shipping.*)

5.5.2 Only for traveling setups

- Design and manufacturing

  ☐Consists of standard equipment supplied by a manufacturer

  ☒CERN/collaboration responsible for the design and/or manufacturing. ISIEC file of eMIL can be found at EDMS: 1317710.

- Describe the hazards generated by the experiment:

Domain	Hazards/Hazardous Activities		Description
Mechanical Safety	Pressure	☐	[pressure] [bar], [volume][l]
	Vacuum	☒	10^{-5} mbar
	Machine tools	☒	The alignment of eMIL with the GLM beam line requires the adjustment of the equipment height.
	Mechanical energy (moving parts)	☒	Stepping motor of four-positions lid.
	Hot/Cold surfaces	☒	Cold surface for liquid N_2 experiments. Hot lid does not cause hot surface.
Cryogenic Safety	Cryogenic fluid	☒	Liquid N_2 (approximately 4 liters per load)
Electrical Safety	Electrical equipment and installations	☒	Several devices, please consult the safety file

			EDMS 1317710 for details.
	High Voltage equipment	☒	Detector 1000 V DC with current being less than 1 nA.
Chemical Safety	CMR (carcinogens, mutagens and toxic to reproduction)	☐	[fluid], [quantity]
	Toxic/Irritant	☐	[fluid], [quantity]
	Corrosive	☐	[fluid], [quantity]
	Oxidizing	☐	[fluid], [quantity]
	Flammable/Potentially explosive atmospheres	☐	[fluid], [quantity]
	Dangerous for the environment	☐	[fluid], [quantity]
Non-ionizing radiation Safety	Laser	☐	[laser], [class]
	UV light	☐	
	Magnetic field	☒	0.6 T
Workplace	Excessive noise	☒	General ISOLDE hall background noise.
	Working outside normal working hours	☒	According to the ISOLDE schedule.
	Working at height (climbing platforms, etc.)	☐	
	Outdoor activities	☐	
Fire Safety	Ignition sources	☐	
	Combustible Materials	☐	
	Hot Work (e.g. welding, grinding)	☒	Measurements of samples using the hot lid (cold surface).
Other hazards	^{57}Mn (high-energy beta emitter) ^{119}In (activity of the online experiment could be high and should be supervised by radiation protection)		